



NUMERICAL MODELLING OF THE PROPAGATION OF UNDERWATER ACOUSTIC WAVES

José A. F. Santiago*

Luiz C. Wrobel

Brunel University - Department of Mechanical Engineering
Uxbridge, Middlesex - UB8 3PH - England

* On leave from COPPE/Federal University of Rio de Janeiro, Brazil

***Abstract .** This paper deals with the numerical simulation of acoustic wave propagation in shallow water by the boundary element method. It is assumed that the source of acoustic disturbance is time-harmonic, the velocity of sound is constant and the medium in the absence of perturbations is quiescent.*

For regions of constant depth, the boundary condition on the free surface and bottom boundaries is incorporated into the Green's function, obtaining fundamental solutions in the form of infinite series. Therefore, only irregular bottom boundaries need to be discretized. A simple numerical test is included to validate the formulation.

Key words: Acoustic, Boundary Elements, Shallow Water

1. INTRODUCTION

Increasing concern for coastal areas has, in recent years, focussed studies of ocean acoustic wave propagation on shallow water environments. The most common numerical techniques used to model underwater acoustic wave propagation are ray methods, normal mode methods, and parabolic equation methods (Jensen et al., 1994). Ray methods are used in deep water and are restricted to high frequencies; normal mode methods are best suited for low frequencies but experience difficulties with domains that are both range and depth dependent; parabolic equation methods neglect backscattering effects which are likely to be important in very shallow water and near the shore (Grilli et al, 1998).

The present paper proposes a novel boundary element formulation for the numerical modelling of shallow water acoustic propagation, in the frequency domain, over irregular bottom topography. The model assumes a two-dimensional geometry, representative of coastal regions, which have little variation in the long shore direction. The boundary element method (BEM) model makes use of a Green's function which directly satisfies the boundary conditions at the free surface and the horizontal part of the bottom surface. Therefore, only bottom irregularities need to be discretized.

The BEM formulation has been implemented and tested with several problems with simple geometries. Results of some such tests are included to assess the accuracy of numerical solutions.

2. BOUNDARY ELEMENT METHOD

Two typical cases of 2D shallow water problems can be seen in Figure 1. The first corresponds to those with one open boundary, representing ocean sections near coastal regions, while the second corresponds to those with two open boundaries, representing ocean sections far from the shore.

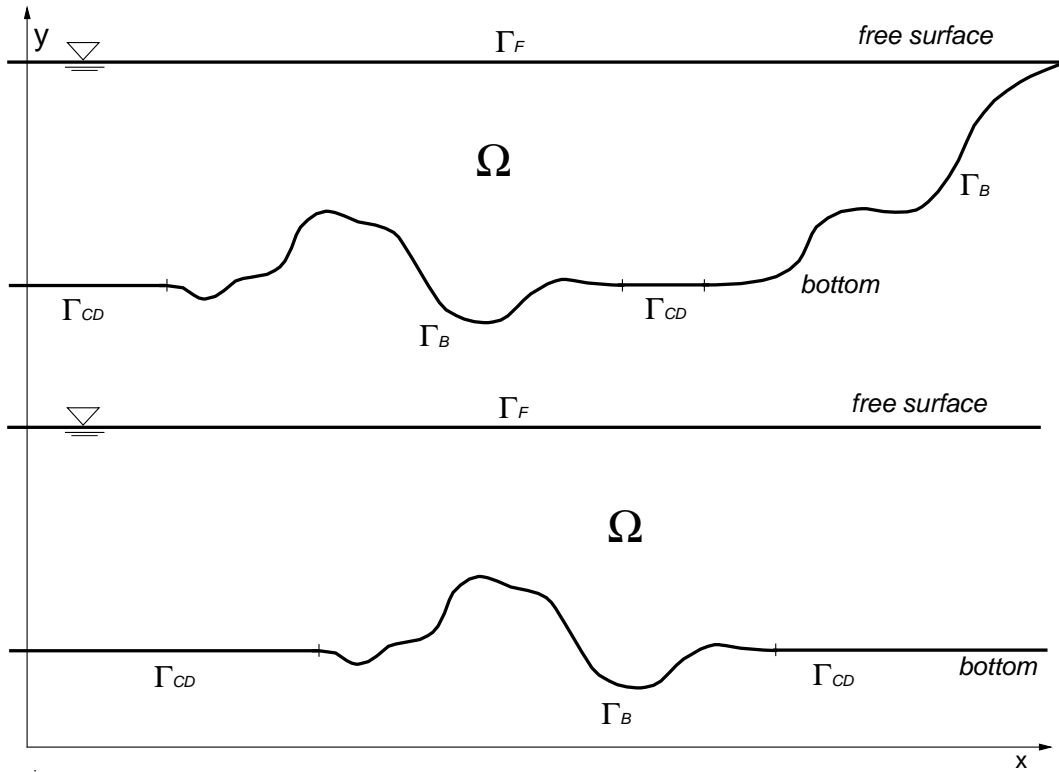


Figure 1 – General ocean sections for 2D acoustic propagation problems in shallow water

Consider the problem of acoustic wave propagation in a volume Ω of infinite extent, shown in Figure 1. Assuming that this medium in the absence of perturbations is quiescent, the velocity of sound is constant and the source of acoustic disturbance is time-harmonic, the problem is governed by the Helmholtz equation (Kinsler et al,1982):

$$\nabla^2 u + k^2 u = -\sum_{\alpha=1}^{Nes} B_{\alpha} \delta(\mathbf{E}_{\alpha}, \mathbf{S}) \quad \text{in } \Omega \quad (1)$$

where u is the velocity potential, B_{α} is the magnitude of the exciting source \mathbf{E}_{α} located at $(x_{e_{\alpha}}, y_{e_{\alpha}})$, \mathbf{S} is the source point, Nes is the number of exciting sources, $\delta(\mathbf{E}_{\alpha}, \mathbf{S})$ is the Dirac delta generalised function and $k = w/c$ is the wave number, in which w is the natural frequency and c is the velocity of sound in the medium.

The problem is subject to the following boundary conditions:

a) Dirichlet condition

$$u(\mathbf{X}) = 0 \quad \text{on } \Gamma_F \quad (2a)$$

b) Neumann condition

$$\frac{\partial u}{\partial n}(\mathbf{X}) = 0 \quad \text{on } \Gamma_{CD} \text{ and } \Gamma_B \quad (2b)$$

c) Sommerfeld radiation condition at infinity

$$\frac{\partial u}{\partial n}(\mathbf{X}) = iku(\mathbf{X}) \quad (2c)$$

in which Γ_F , Γ_B and Γ_{CD} are the free surface, irregular bottom and constant depth bottom, respectively (see Figure 1), n is the outward normal vector and $i = \sqrt{-1}$.

According to Green's second identity, Eq. (1) can be transformed into the following boundary integral equation (Chen and Zhou, 1992; Lacerda, 1997)

$$c(\mathbf{S})u(\mathbf{S}) = \int_{\Gamma} G(\mathbf{S}, \mathbf{X}) \frac{\partial u}{\partial n}(\mathbf{X}) d\Gamma - \int_{\Gamma} \frac{\partial G}{\partial n}(\mathbf{S}, \mathbf{X}) u(\mathbf{X}) d\Gamma + \sum_{\alpha=1}^{Nes} B_{\alpha} G(\mathbf{E}_{\alpha}, \mathbf{S}) \quad (3)$$

where Γ is equal to $\Gamma_F \cup \Gamma_B \cup \Gamma_{CD}$, \mathbf{S} and \mathbf{X} are the source and field points, respectively and $G(\mathbf{S}, \mathbf{X})$ is the Green's function. The functions $u(\mathbf{X})$ and $\partial u/\partial n(\mathbf{X})$ represent the velocity potential and its normal derivative. The coefficient $c(\mathbf{S})$ depends on the boundary geometry at the source point \mathbf{S} . It is noted that the Green's function implicitly satisfies the Sommerfeld condition, therefore no discretization of the boundary at infinity is necessary.

Instead of using the fundamental solution (free-space Green's function) of the Helmholtz equation, modified Green's functions which directly satisfy the boundary conditions on Γ_F and Γ_{CD} are adopted. Therefore, only the irregular parts of the bottom boundary, denoted by Γ_B in Figure 1, need to be discretized. These fundamental solutions are developed using the method of images, and have the form of infinite series:

$$G_F(\mathbf{S}, \mathbf{X}) = i \frac{1}{4} \left\{ H_0^{(1)}(kr) - H_0^{(1)}(kr^{(1F)}) + \sum_{m=1}^{\infty} (-1)^{m+1} \left[H_0^{(1)}(kr_m^{(2F)}) - H_0^{(1)}(kr_m^{(3F)}) \right] \right. \\ \left. - H_0^{(1)}(kr_m^{(4F)}) + H_0^{(1)}(kr_m^{(5F)}) \right\} \quad (4)$$

$$\frac{\partial G_B}{\partial n}(\mathbf{S}, \mathbf{X}) = -i \frac{k}{4} \left\{ H_1^{(1)}(kr) \frac{\partial r}{\partial n} + H_1^{(1)}(kr^{(1B)}) \frac{\partial r^{(1B)}}{\partial n} \right. \\ \left. + \sum_{m=1}^{\infty} (-1)^m \left[H_1^{(1)}(kr_m^{(2B)}) \frac{\partial r_m^{(2B)}}{\partial n} + H_1^{(1)}(kr_m^{(3B)}) \frac{\partial r_m^{(3B)}}{\partial n} \right] \right. \\ \left. + H_1^{(1)}(kr_m^{(4B)}) \frac{\partial r_m^{(4B)}}{\partial n} + H_1^{(1)}(kr_m^{(5B)}) \frac{\partial r_m^{(5B)}}{\partial n} \right\} \quad (5)$$

where $H_0^{(1)}(\)$ and $H_1^{(1)}(\)$ are Hankel functions of the first kind, of order 0 and 1, respectively. The modified Green's function G_F exactly satisfies the boundary condition on the free surface, but its normal derivative produces a small non-zero value at the bottom boundary. Alternatively, function G_B produces a small non-zero value at the free surface but its normal derivative exactly satisfies the boundary condition on the bottom. The above combination, Eq. (4) and (5), was implemented in the present work.

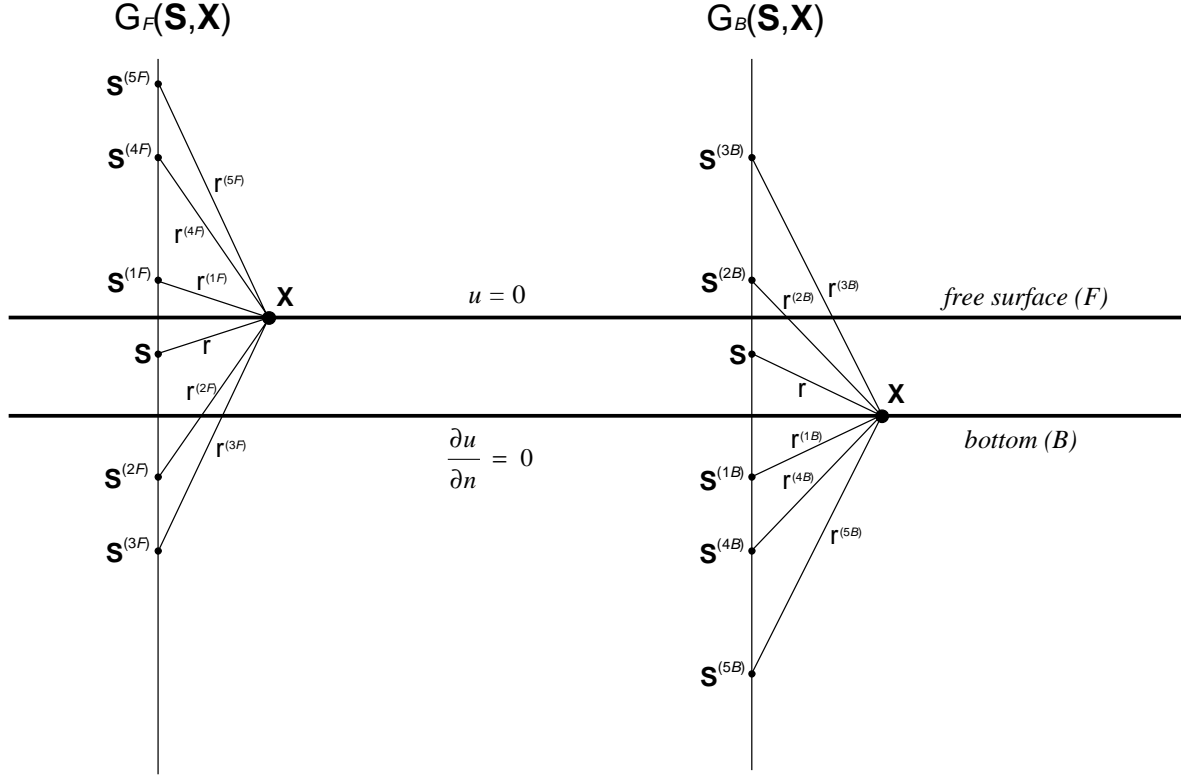


Figure 2 – Distance from field point \mathbf{X} to source point \mathbf{S} and its reflections with respect to free surface and bottom

The distances from the source point \mathbf{S} and its reflections (see Figure 2) to field point \mathbf{X} are denoted as r , $r^{(1F)}$ and $r_m^{(jF)}$ for G_F . These distances can be written as:

$$r = |\mathbf{X} - \mathbf{S}| = \sqrt{(x - x_s)^2 + (y - y_s)^2} \quad (6)$$

$$r^{(1F)} = |\mathbf{X} - \mathbf{S}^{(1F)}| = \sqrt{(x - x_s)^2 + [y - (2Y_F - y_s)]^2} \quad (7)$$

$$r_m^{(jF)} = |\mathbf{X} - \mathbf{S}^{(jF)}| = \sqrt{(x - x_s)^2 + (y - y_m^{(jF)})^2}, \quad j = 2, 3, 4 \text{ and } 5 \quad (8)$$

with:

$$y_m^{(2F)} = -2(m-1)Y_F + 2mY_B - y_s \quad (9a)$$

$$y_m^{(3F)} = 2m(-Y_F + Y_B) + y_s \quad (9b)$$

$$y_m^{(4F)} = 2m(Y_F - Y_B) + y_S \quad (9c)$$

$$y_m^{(5F)} = 2(m+1)Y_F - 2mY_B - y_S \quad (9d)$$

Equations (6) to (9) are also used for G_B , but the letter F must be replaced by B and vice-versa. In these equations, Y_F and Y_B are y co-ordinates of the free surface and bottom, respectively.

Introducing the boundary conditions $u = 0$ on the free surface and $\partial u / \partial n = 0$ on the bottom in Eq.(3) yields

$$c(\mathbf{S})u(\mathbf{S}) = - \int_{\Gamma_B} \frac{\partial G_B}{\partial n}(\mathbf{S}, \mathbf{X})u(\mathbf{X})d\Gamma + \sum_{\alpha=1}^{Nes} B_\alpha G_F(\mathbf{E}_\alpha, \mathbf{S}) \quad (10)$$

In order to solve Eq. (10) numerically, the boundary Γ_B is discretized into a number of boundary elements whose geometries are modelled through shape functions and geometrical nodal points. Over these elements, the velocity potential is interpolated as a function of the element nodal points. Constant elements with linear geometry have been used in this work.

Applying the collocation method to Eq. (10) gives, in terms of an intrinsic co-ordinate η

$$c(\mathbf{S}_p)u(\mathbf{S}_p) + \sum_{q=1}^{ne} u_q \frac{L_q}{2} \int_{-1}^{+1} \frac{\partial G_B}{\partial n}(\mathbf{S}_p, \mathbf{X}_q)d\eta = \sum_{\alpha=1}^{Nes} B_\alpha G_F(\mathbf{E}_\alpha, \mathbf{S}_p) \quad (11)$$

$p = 1, \dots, nf$

where nf is the total number of functional nodes, ne is the number of elements (for constant elements $nf = ne$), \mathbf{S}_p are selected points which coincide with the functional nodal points, L_q is the length of element Γ_q and u_q is the velocity potential at the point \mathbf{X}_q which is the mid-point of element Γ_q .

Applying Eq. (11) to all functional nodal points yields

$$\mathbf{H} \mathbf{u} = \mathbf{b} \quad (12)$$

where vector \mathbf{b} contains the contribution of the exciting sources and matrix \mathbf{H} contains the influence coefficients,

$$H_{pq} = \frac{L_q}{2} \int_{-1}^{+1} \frac{\partial G_B}{\partial n}(\mathbf{S}_p, \mathbf{X}_q)d\eta + \frac{1}{2} \delta_{pq} \quad (13a)$$

$$b_p = \sum_{\alpha=1}^{Nes} B_\alpha G_F(\mathbf{E}_\alpha, \mathbf{S}_p) \quad (13b)$$

where δ_{pq} is the Kronecker delta.

The number of terms necessary for evaluation of the series G_F and $\partial G_B / \partial n$ is decided based upon the following procedures:

a) To calculate the series G_F :

The sum of terms for the m -th iteration is obtained as

$$H_m^{(F)}(\mathbf{E}_\alpha, \mathbf{S}_p) = H_0^{(1)}(kr_m^{(2F)}) - H_0^{(1)}(kr_m^{(3F)}) - H_0^{(1)}(kr_m^{(4F)}) + H_0^{(1)}(kr_m^{(5F)}) \quad (14a)$$

with

$$r_m^{(jF)} = |\mathbf{S}_p - \mathbf{E}_\alpha^{(jF)}| \quad (14b)$$

where $\mathbf{E}_\alpha^{(jF)}$ is the reflection $\mathbf{E}^{(jF)}$ of the exciting source \mathbf{E}_α .

The process will be finished when the influence of this sum $H_m^{(F)}$ into the accumulated term $\sum_{\beta=1}^m H_\beta^{(F)}$ satisfies the following inequality:

$$\left| \frac{H_m^{(F)}(\mathbf{E}_\alpha, \mathbf{S}_p)}{\sum_{\beta=1}^m H_\beta^{(F)}(\mathbf{E}_\alpha, \mathbf{S}_p)} \right| < Tol \quad (15)$$

where Tol is the tolerance, the value of which affects the accuracy of calculations.

b) To calculate the series $\partial G_B / \partial n$:

The integral in Eq. (13a) is computed numerically using Gaussian quadrature for either the complete series or term by term. In the first case, the number of Gauss points must be the same for terms with small and large r , increasing the computer time. A term by term integration with different number of Gauss points has been used. In addition, only one Gauss point is employed to integrate terms with source point reflection far from the bottom and free surface. Therefore, the sum of terms for m -th iteration is obtained as

$$\begin{aligned} H_m^{(B)}(\mathbf{S}_p, \mathbf{X}_q) = & \int_{-1}^{+1} H_1^{(1)}(kr_m^{(2B)}) \frac{\partial r_m^{(2B)}}{\partial n} d\eta + \int_{-1}^{+1} H_1^{(1)}(kr_m^{(3B)}) \frac{\partial r_m^{(3B)}}{\partial n} d\eta \\ & + \int_{-1}^{+1} H_1^{(1)}(kr_m^{(4B)}) \frac{\partial r_m^{(4B)}}{\partial n} d\eta + \int_{-1}^{+1} H_1^{(1)}(kr_m^{(5B)}) \frac{\partial r_m^{(5B)}}{\partial n} d\eta \end{aligned} \quad (16a)$$

with

$$r_m^{(jB)} = |\mathbf{X}_q - \mathbf{S}_p^{(jB)}| \quad (16b)$$

where $\mathbf{S}_p^{(jB)}$ is the reflection $\mathbf{S}^{(jB)}$ of the source point \mathbf{S}_p .

Now, the process will be terminated when the influence of this sum $H_m^{(B)}$ into the accumulated term $\sum_{\beta=1}^m H_\beta^{(B)}$ satisfies a similar inequality:

$$\left| \frac{H_m^{(B)}(\mathbf{S}_p, \mathbf{X}_q)}{\sum_{\beta=1}^m H_\beta^{(B)}(\mathbf{S}_p, \mathbf{X}_q)} \right| < Tol \quad (17)$$

3. APPLICATION

A simple application is presented here to validate the fundamental solutions through the behaviour of the velocity potential along the bottom and at selected internal points.

This example simulates the propagation of acoustic waves into infinite shallow water with a rectangular obstacle. The analysis is two-dimensional as shown in Figure 3. The deeper and shallower depths are equal to h (in metre), and $h/2$, respectively. The velocity of sound and the frequency are taken to be 1500 m/s and 7500 rad/s, respectively. The magnitude of the exciting source is equal to $1.0 \text{ m}^2/\text{s}$ and it is located at $x_E = 10h$ and $y_E = h/2$.

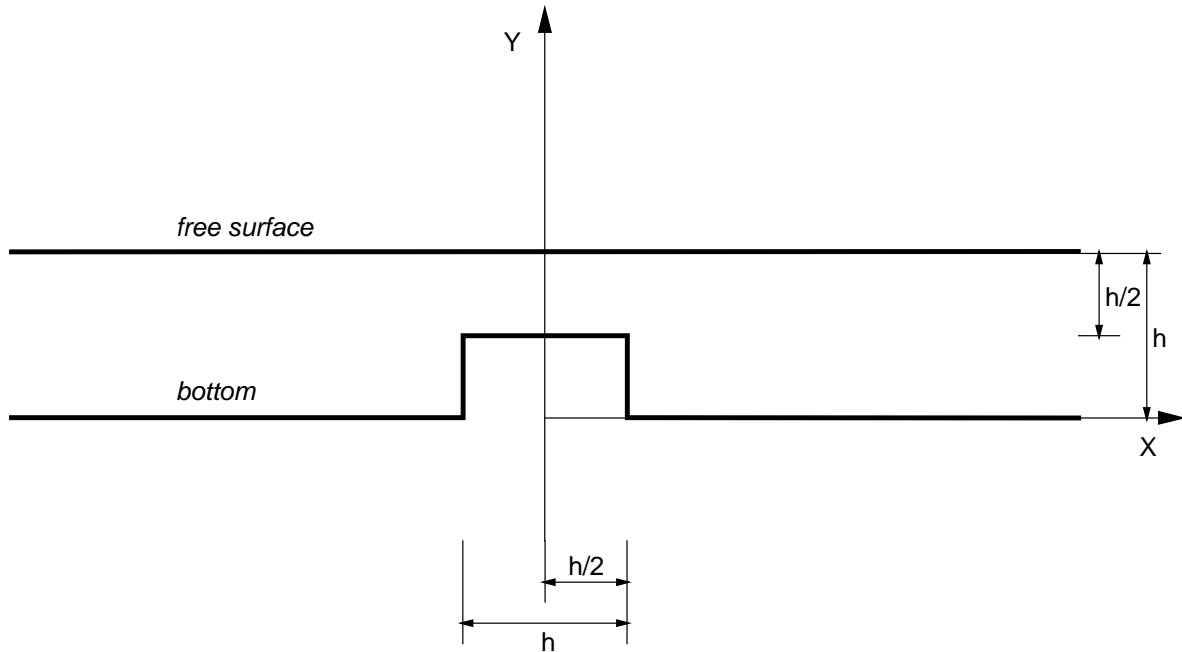


Figure 3 – Geometry for rectangular obstacle on the seabed

The boundary conditions and element discretization are depicted in Figure 4. A rigid bottom is adopted, hence $\frac{\partial u}{\partial n} = 0$ for all functional nodal points. Only the rectangular obstacle is discretized with constant elements of the same length in three different meshes. The first has 5 and 10 elements on the vertical and horizontal sides, respectively, while the others have 10/20 and 20/40 elements.

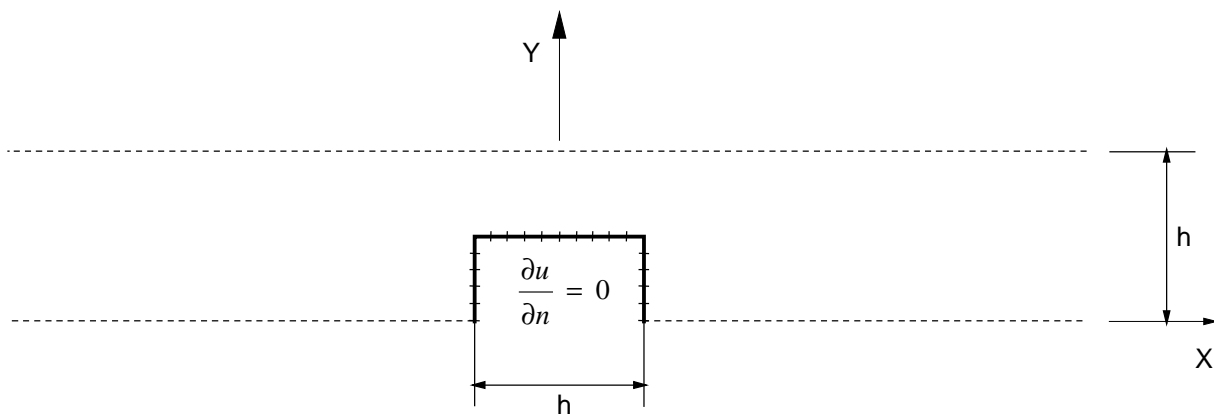


Figure 4 – Discretization and boundary conditions of the problem

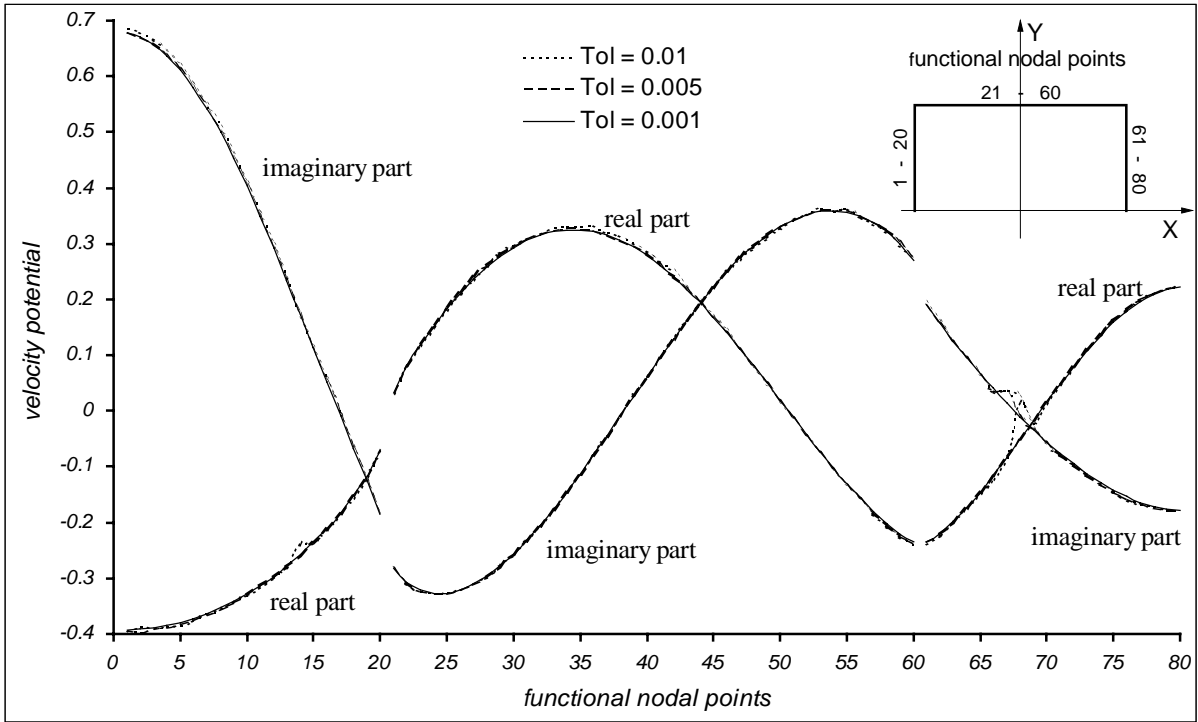


Figure 5 – Velocity potential at functional nodal points on the boundary of the rectangular obstacle for different tolerances (Tol)

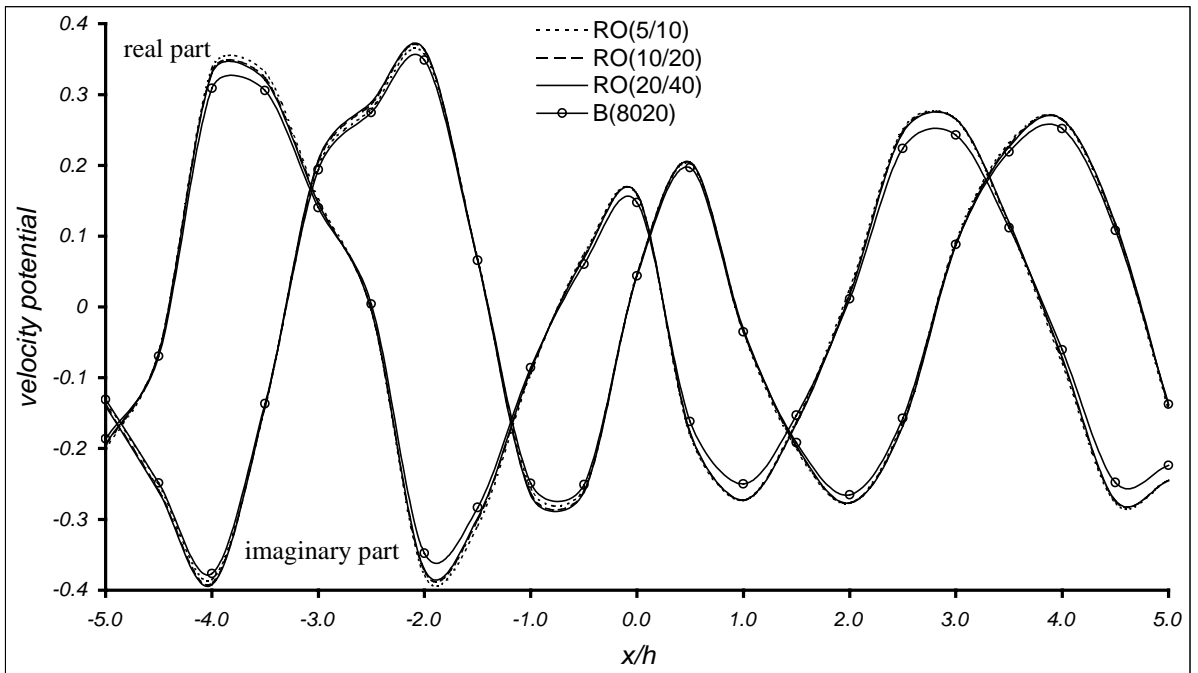


Figure 6 – Velocity potential at internal points along the horizontal line $y = 0.8h$
 RO(elements): discretized rectangular obstacle only B(elements): discretized bottom

Figure 5 shows the velocity potential at the functional nodal points on the rectangular obstacle for different tolerances, using a mesh of 20 and 40 elements on the sides. As can be seen, for the tolerance of 0.001 the curve is all smooth, whereas there are small local perturbations for higher values of tolerance.

In order to assess the accuracy of the results, the problem was also analysed with an alternative BEM formulation in which the bottom boundary is fully discretized but the free surface is eliminated using a single image source. The infinite bottom boundary was truncated at the distances $-500h$ and $+500h$.

To observe the behaviour of the velocity potential at internal points, analyses were carried out using the BEM with infinite series and single image source. The first uses the same tolerance of 0.001 for different meshes of 5/10, 10/20 and 20/40 elements on the vertical/horizontal sides of the obstacle. The second analysis employs 8020 elements to discretize the bottom, with 8000 elements along the infinite boundary (10 elements per wavelength) and 5/10 on the obstacle. Results for the velocity potential at internal points along the horizontal line $y = 0.8h$ and over the vertical $x = -0.5h$ are presented in Figures 6 and 7.

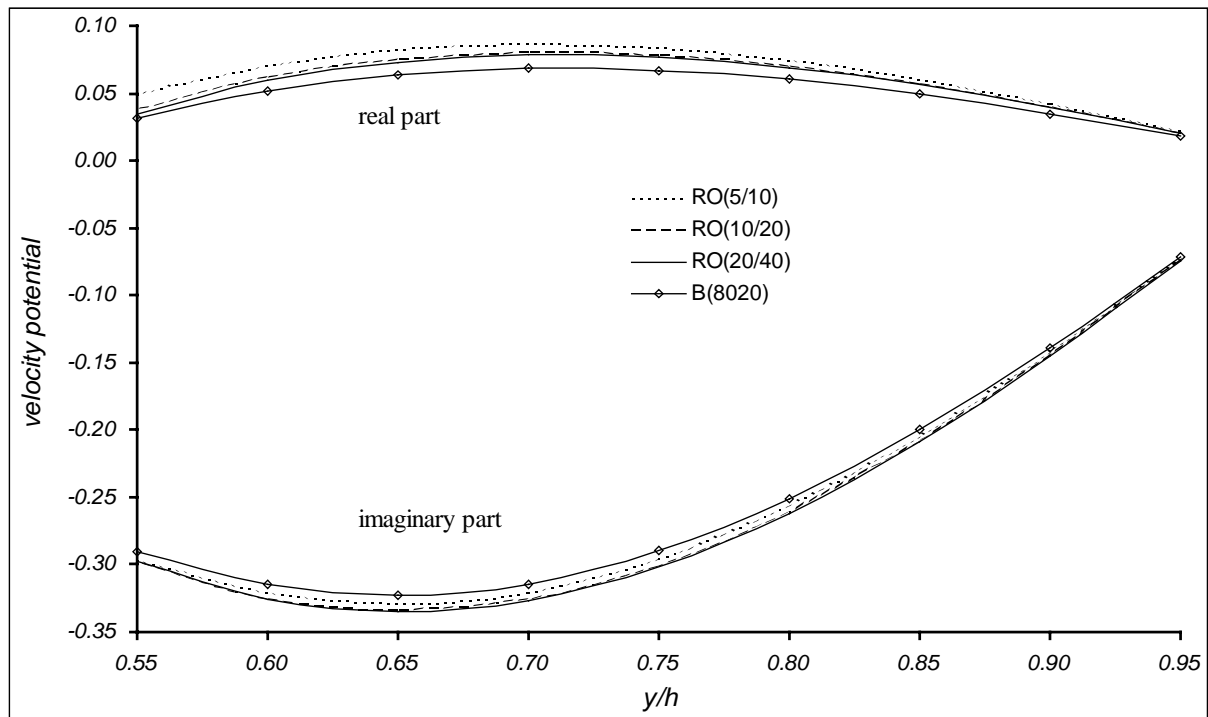


Figure 7 – Velocity potential at internal points along the vertical line $x = -0.5h$
 RO(elements): discretized rectangular obstacle only B(elements): discretized bottom

4. CONCLUSION

The infinite series employed as fundamental solutions were initially validated for simple geometries for which analytic solutions are known. These series were then implemented in a BEM computer program and produced excellent results for the test cases carried out. It is observed that the choice of tolerance and number of nodes per wavelength affect the behaviour of the velocity potential. Therefore, the value adopted for tolerance should be small enough to avoid local perturbations of the results.

The convergence of the developed infinite series is very slow and studies have been elaborated in order to improve upon this by finding out alternative series and modifying the calculation of the asymptotic form of the Hankel function when source points are far from the free surface and bottom.

Acknowledgement

The first author would like to thank CNPq, the Brazilian Research Council, for providing financial support to this research.

REFERENCES

Chen, G. and Zhou, J., 1992, *Boundary Element Methods*, Academic Press, UK.

Grilli, S., Pedersen, T. and Stepanishen, P., 1998, A hybrid boundary element method for shallow water acoustic propagation over an irregular bottom, *Engineering Analysis with Boundary Elements*, 21, 131-145.

Jensen, F. B., Kuperman, W. A., Porter, M. B. and Schmidt, H., 1994, *Computational Ocean Acoustics*, American Institute of Physics, USA.

Kinsler, L.E., Frey, A.R., Coppens, A.B and Sanders, J.V., 1982, *Fundamentals of Acoustics*, Third edition, John Wiley & Sons, USA.

Lacerda; L.A. de, 1997, *Boundary element formulations for outdoor sound propagation* (in Portuguese), D.Sc. Thesis, Department of Civil Engineering, COPPE/UFRJ, Brazil.